
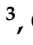







Article

Development and Investigation of Photoactive WO₃ Nanowire-Based Hybrid Membranes

Mohammed Ahmed Shehab ^{1,2}, Nikita Sharma ³, Gábor Karacs ⁴, Lilla Nánai ⁵, István Kocserha ⁶, Klara Hernadi ^{5,*} and Zoltán Németh ^{3,*}

- ¹ Faculty of Materials and Chemical Engineering, University of Miskolc, H-3515 Miskolc, Hungary
² Polymers and Petrochemicals Engineering Department, Basrah University for Oil and Gas, Basrah 61004, Iraq
³ Advanced Materials and Intelligent Technologies Higher Education and Industrial Cooperation Centre, University of Miskolc, H-3515 Miskolc, Hungary
⁴ ELKH-ME Materials Science Research Group, ELKH, University of Miskolc, H-3515 Miskolc, Hungary
⁵ Institute of Physical Metallurgy, Metal Forming and Nanotechnology, University of Miskolc, H-3515 Miskolc, Hungary
⁶ Institute of Ceramics and Polymer Engineering, University of Miskolc, H-3515 Miskolc, Hungary
* Correspondence: femhernadi@uni-miskolc.hu (K.H.); kemnemet@uni-miskolc.hu (Z.N.)

Abstract: Novel hybrid structures have attracted attention in several instances of scientific research and different technological applications in this decade due to their novel characteristics and wide range of applicability. Hybrid membranes with multiple components (three or more) are also increasingly used in water purification applications, and their ease of handling and reusability make them a promising candidate for the degradation of organic pollutants by photocatalysis. In this study, the preparation and characterization of tungsten trioxide nanowire (WO₃ NW)-based hybrid membrane structures are reported. Furthermore, the adsorption properties and photocatalytic efficiency of the as-prepared membranes against methylene blue (MB) organic dye under UV irradiation is also presented. Characterization techniques, such as scanning electron microscopy (SEM), high-resolution transmission electron microscopy (HRTEM), energy-dispersive X-ray spectroscopy (EDS), and X-ray powder diffraction (XRD) are performed to study the morphology and surface of the as-prepared hybrid membranes. The removal efficiency of the hybrid membranes against MB is 77% in a 120 min decomposition reaction. The enhanced value can be attributed to the hybrid structure of the membrane that enhances not only the adsorption capability, but also the photocatalytic performance. Based on the results obtained, it is hoped that hybrid membrane technology could be a promising candidate for future photocatalysis-based water treatment applications.

Keywords: hybrid membrane preparation; electron microscopy; photocatalysis; organic dye decomposition



Citation: Shehab, M.A.; Sharma, N.; Karacs, G.; Nánai, L.; Kocserha, I.; Hernadi, K.; Németh, Z. Development and Investigation of Photoactive WO₃ Nanowire-Based Hybrid Membranes. *Catalysts* **2022**, *12*, 1029. <https://doi.org/10.3390/catal12091029>

Academic Editors: Shou-Heng Liu and Ying-Chih Pu

Received: 27 July 2022

Accepted: 6 September 2022

Published: 10 September 2022

Publisher's Note: MDPI stays neutral with regard to jurisdictional claims in published maps and institutional affiliations.



Copyright: © 2022 by the authors. Licensee MDPI, Basel, Switzerland. This article is an open access article distributed under the terms and conditions of the Creative Commons Attribution (CC BY) license (<https://creativecommons.org/licenses/by/4.0/>).

1. Introduction

The growing world population has led to a respective increase in environmental pollution and energy needs. This has become a severe problem globally due to the negative effects on drinking water, soil, human and animal health caused by the presence of pollutants. There are concerns due to the uncontrolled discharge of industrial wastewater, which mainly comprises organic pollutants, including dyes, industrial chemicals, pesticides, microplastics and pharmaceutical waste [1–4].

A large amount of research has been performed in the field of water purification studies to develop appropriate and sustainable methods and technologies to remove the above-described pollutants from water. A range of conventional physical water treatment techniques, such as adsorption, coagulation, filtration, reverse osmosis, etc., have been applied for the removal of pollutants, but these techniques have faced specific limitations which have made them ineffective in eliminating the targeted contaminants from the

water [5,6]. This can be confirmed by the fact that the majority of these contaminants can be still found in reasonable concentrations in the water that has undergone these physical treatments.

For such reasons, there has been significant interest in some advanced oxidation processes, such as homogenous and heterogenous photocatalysis, photoelectrocatalytic oxidation, etc. Over the years, heterogenous photocatalysis has been given particular prominence as a potential wastewater treatment alternative, with specific interest in TiO₂ as the main semiconductor photocatalyst, which has been used in the degradation of a wide range of organic, and a few inorganic, pollutants. TiO₂-based photocatalysts have gained tremendous attention due to their beneficial features, for instance, being chemically stable, low cost and non-toxic, but the major setback of TiO₂ is that it is unable to harness visible light due to its wide bandgap (3.2 eV) [7]. As a result, the efficiency of visible-light-spectrum utilization is low and TiO₂ shows a low photocatalytic efficiency due to the rapid recombination of photogenerated electron-hole pairs and poor photoinduced reaction performance [8]. The photoactivity of TiO₂ is significant in UV light; therefore, UV lamps are required to maximize the elimination of targeted pollutants, which results in higher operating costs.

In recent years, semiconductors with smaller bandgap energy (<3.0 eV) have been investigated, and they have appeared promising with an efficient harnessing of visible light from the solar spectrum [9]. Some of these semiconductors include silver orthophosphate (Ag₃PO₄) (~2.4 eV) [10], bismuth oxyhalides (BiOX, X = Br, Cl, and I) (1.77–3.5 eV) [11–13], graphitic carbon nitride (g-C₃N₄) (2.7 eV) [14], tungsten trioxide (WO₃) [15–17], etc., and their composites. WO₃-based photocatalysts are one of the most important metal oxide groups as visible-light-active n-type semiconductor photocatalysts, and they have gained major attention due to their narrow bandgaps (2.4–2.8 eV); outstanding physical, chemical and optical properties; large surface area; resistance to chemicals and photocorrosion; low toxicity; and low costs [18–20].

Synthesis methods play a crucial role in the preparation of photocatalysts. The photocatalytic activity depends on various factors. Many attempts have been made to control the size distribution and the structure and dimensionality of nanocatalysts because these are regarded as the key parameters affecting their photocatalytic performance. Various synthesis approaches can be used to synthesize photocatalysts with different morphologies, properties, structures, and sizes, and are mainly responsible for enhanced photocatalytic performance [9,19]. Widely used methods for the preparation of WO₃ and WO₃-based photocatalysts are hydrothermal [21,22], solvothermal [23,24], sol-gel [22,25,26], co-precipitation [27,28] and “green synthesis” [17,29–31] methods, the last of which is considered as a new and promising method. In order to enhance the photocatalytic efficiency, a large and specific surface area is beneficial; therefore, in recent years, researchers have focused on studying WO₃ nanomaterials such as nanoparticles (NP), nanorods and nanowires (NW). These nanofibers have high surface-to-volume ratios; thus, they also have increased photocatalytic performance. In some studies, WO₃ NWs have shown much higher photocatalytic efficiency due to their high aspect ratio, compared to WO₃ NPs [32].

The photocatalytic degradation of methylene blue (MB) over semiconductor photocatalysts under UV light involves photo-exciting by photons, leading to a release of electrons from valence band (VB) to conduction band (CB). This process generates a hole (h⁺) in VB that results in an electron-hole pair, the h⁺ reacting with water to produce the free radical OH[•], which is a strong oxidant agent. On the other hand, the electrons bind with water molecules to produce hydroxyl radicals. At the same time, it is trapped by the oxygen molecules, producing superoxide radicals (O₂^{•−}). These radicals play an important role in oxidation and inhibit electron-hole pair recombination, leading to the regeneration of photocatalysts [33,34].

As with many other semiconductors, the WO₃ photocatalyst has its own restrictions as well, such as the rapid recombination of photogenerated electron-hole pairs. It also has a more positive conduction band level than the O₂/O₂^{•−} reduction potential, which

causes fewer O_2 molecules to be reduced as superoxide anion free radicals ($O_2^{\bullet-}$) during the photocatalytic process [17]. In order to solve the above-mentioned setbacks, numerous methods, such as morphology control [35], heterojunction, construction of hybrid materials [36], and the doping of metal (transition, noble) and non-metal ions [37] have been reported. Among these methods, heterojunctions and the construction of heterostructures have been widely used to enhance the photocatalytic performance and to regulate the bandgap structures. Copper and iron, and their oxides, are extensively used as sensitizer materials to modify the photocatalytic performance of the catalysts by narrowing their bandgap energy, extending the photoabsorption range, enhancing the separation of electron-hole pairs with photoexcitation, and improving the activity in the visible-light range [36,38–40].

Over the years, membrane techniques have become one of the most effective technologies for water treatment due to their small footprint, superior separation efficiency and easy maintenance. During the traditional membrane processes, the pores become clogged due to the contaminations and the formation of cake layers on the membrane surface, which results in a major decrease in water flux, and increased energy consumption that leads to significant treatment costs [41]. Moreover, these filtration methods can only concentrate the pollutants on their surfaces, which need further post-treatment before releasing purified water. For such reasons, photocatalytic membrane (PM) processes could be the solution to degrade the pollutants in the water by photocatalytic reactions, thus preventing the formation of cake layers on the membrane surface and reducing pore blocking, which can enhance the quality of water treatment. In recent studies, photocatalysts have mainly been combined with a variety of organic, inorganic, and metallic materials as a support for the fabrication of PM [42]. Ceramic, polymer and cellulose-based membranes are getting more popular as membranes due to their specific fibrous structure. Their rich surface-functional groups might be able to have a positive impact on stability, dispersity, surface area, hydrophilicity and morphology [43–45]. The photocatalytic membranes have the benefit of having a physical separation during the filtration process, as well as the degradation of pollutants and the anti-bacterial properties of the WO_3 achieved by photocatalysis in a single unit [41,46,47].

In this study, we aim to develop and investigate a bi-functional, WO_3 nanowire (NW)-based hybrid membrane material which will be able to remove dyes and other pollutants from wastewater via adsorption and photocatalytic reactions. For this purpose, WO_3 NW is synthesized using a hydrothermal synthesis method; then, the as-prepared WO_3 NW is combined with Fe_2O_3 and CuO nanoparticles by a modified impregnation technique. The prepared nanocomposites after calcination are combined with a cellulose solution, and the preparation of WO_3 NW-based hybrid membranes is immobilized onto a polyvinylidene fluoride (PVDF) membrane. Morphological, structural and surface properties of the samples are characterized by scanning electron microscopy (SEM), high-resolution transmission electron microscopy (HRTEM), energy-dispersive X-ray spectroscopy (EDS) and X-ray powder diffractometer (XRD) techniques. The study and demonstration of the photocatalytic properties of the hybrid membranes that have been produced also play an important role in the present study, since the potential photoactivity is essential for the regeneration of membranes in future applications. Therefore, the adsorption properties and the photocatalytic performance of the hybrid membranes are investigated against methylene blue organic dye. The results suggest that nanofiber-based hybrid membranes could provide ecofriendly and sustainable solutions as a possible alternative for wastewater treatment applications.

2. Results

2.1. HRTEM and EDS Analysis of WO_3 NW@ Fe_2O_3 and WO_3 NW@ CuO Nanocomposites

Before the preparation of the hybrid membrane, the pristine WO_3 NW (Figure 1a,b) and the heat-treated WO_3 NW@ Fe_2O_3 and WO_3 NW@ CuO nanocomposites (Figure 1c,d) were investigated by an HRTEM technique. TEM micrographs revealed that the synthesis

of the WO_3 NW, the WO_3 NW@ Fe_2O_3 and the WO_3 NW@ CuO nanocomposites were successful. Furthermore, the nanocomposite structures were rather similar, although the average particle sizes of the Fe_2O_3 and CuO nanoparticles that had adhered to the surface of the WO_3 NW were different, as can be seen in Figure 1c,d. The latter TEM images revealed that inorganic nanoparticles (Fe_2O_3 and CuO) were attached to the surface of the WO_3 NW, and segregated particles could not be observed.

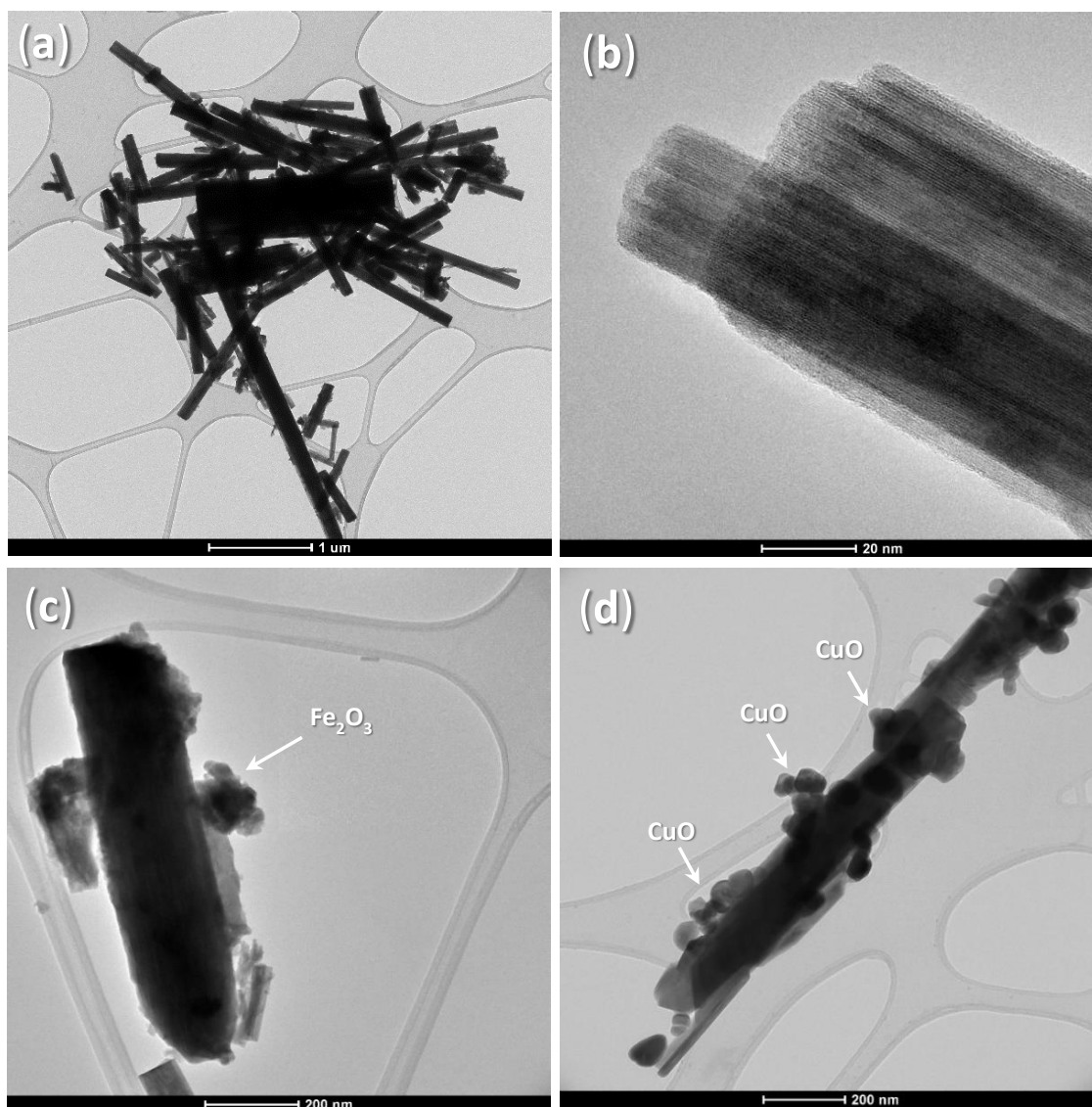


Figure 1. HRTEM images of pristine WO_3 NW (a,b) WO_3 NW@ Fe_2O_3 (c) and WO_3 NW@ CuO (d) nanocomposite samples.

During the HRTEM analysis of the as-prepared WO_3 NW, Fe_2O_3 and CuO nanoparticles were investigated by using the iTEM software (Olympus Soft Imaging Solutions) in order to determine the average diameter of the nanowire and the particle sizes of the nanoparticles. In each case, 100 individual particles were measured. These calculations showed that the WO_3 NW particles had a diameter of 80–100 nm and the average length was estimated as 0.8–3 μm (Figure 1a,b). Based on these calculations, it was found that Fe_2O_3 nanoparticles had diameters in the range of 40–50 nm, as can be seen in Figure 1c, while CuO nanoparticles had diameters between 20 and 30 nm, as can be seen in Figure 1d.

To characterize and identify the composing elements in the WO_3 NW@ Fe_2O_3 and WO_3 NW@ CuO nanocomposites, EDS analysis was performed. Figure 2a,b show the EDS

spectra and confirm the presence of oxygen (O), tungsten (W), iron (Fe) and copper (Cu). These signals originated from the WO_3 NW, and Fe_2O_3 and CuO in the nanocomposites, while the Cu peak—in the case of the WO_3 NW@ Fe_2O_3 nanocomposite sample—originated from the sample holder (Cu grid).

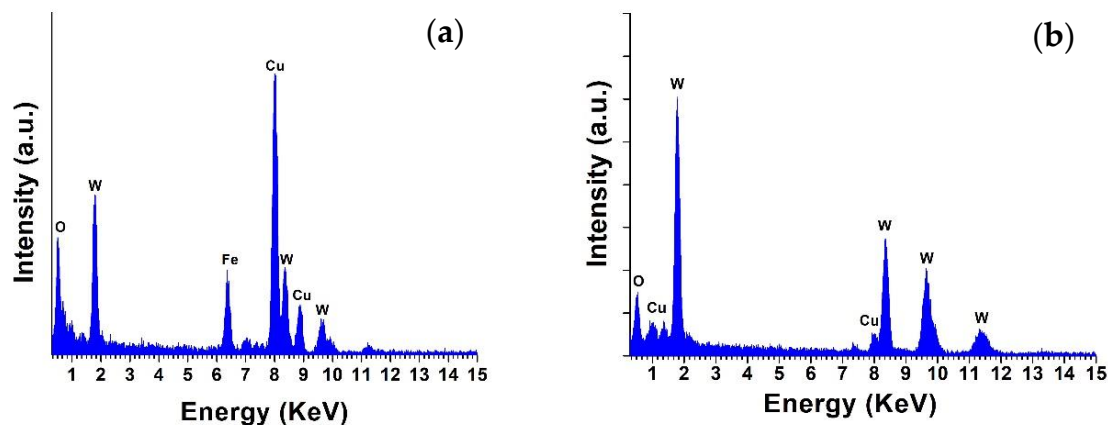


Figure 2. EDS spectra of WO_3 NW@ Fe_2O_3 (a) and WO_3 NW@ CuO (b) nanocomposites.

2.2. SEM and EDS Analysis of WO_3 NW@ Fe_2O_3 /Cellulose and WO_3 NW@ CuO /Cellulose Membranes

To study the surface morphology of the produced WO_3 NW@ Fe_2O_3 /cellulose and WO_3 NW@ CuO /cellulose hybrid membranes, SEM analyses were performed. The morphology of the unmodified WO_3 NW (Figure 3a,b), the as-prepared WO_3 /cellulose (Figure 4a,b), WO_3 NWs@ Fe_2O_3 /cellulose (Figure 4c,d) and WO_3 NWs@ CuO /cellulose hybrid membrane (Figure 4e,f) were investigated.

In the SEM images shown in Figure 3a,b, the average diameter of the WO_3 nanowires is 100–120 nm. The photographs in Figure 4a,c,e show the produced self-supported membranes, while the SEM images in Figure 4b,d,f demonstrate the microstructure of the WO_3 NW/cellulose (Figure 4b), WO_3 NWs@ Fe_2O_3 /cellulose (Figure 4d), and WO_3 NWs@ CuO /cellulose (Figure 4f) hybrid materials. For the WO_3 NWs@ CuO /cellulose membrane, an increased pore size was observed due to the smaller individual particle size of the CuO nanoparticles.

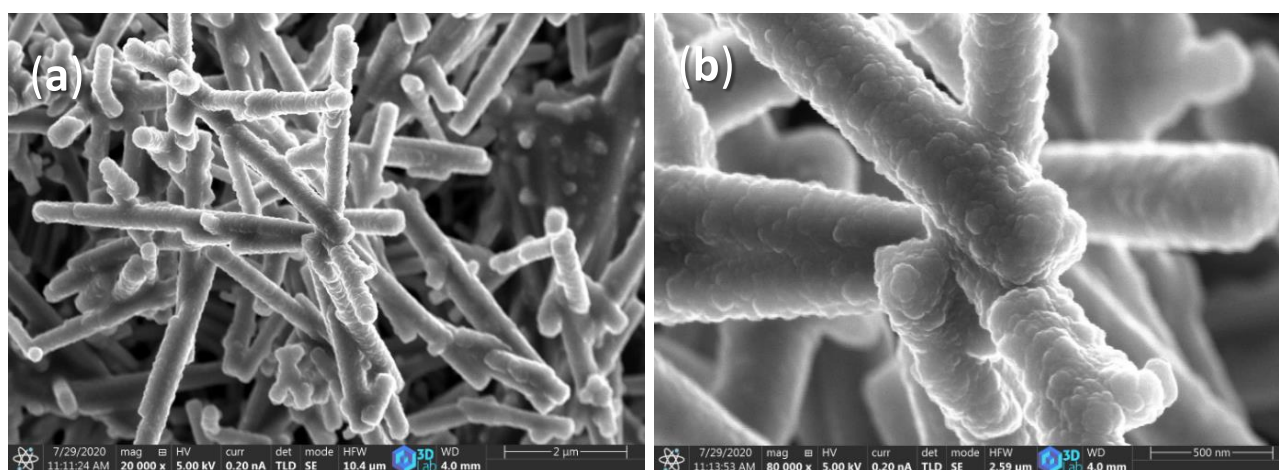


Figure 3. SEM images of WO_3 NW (a) lower and (b) higher magnifications.

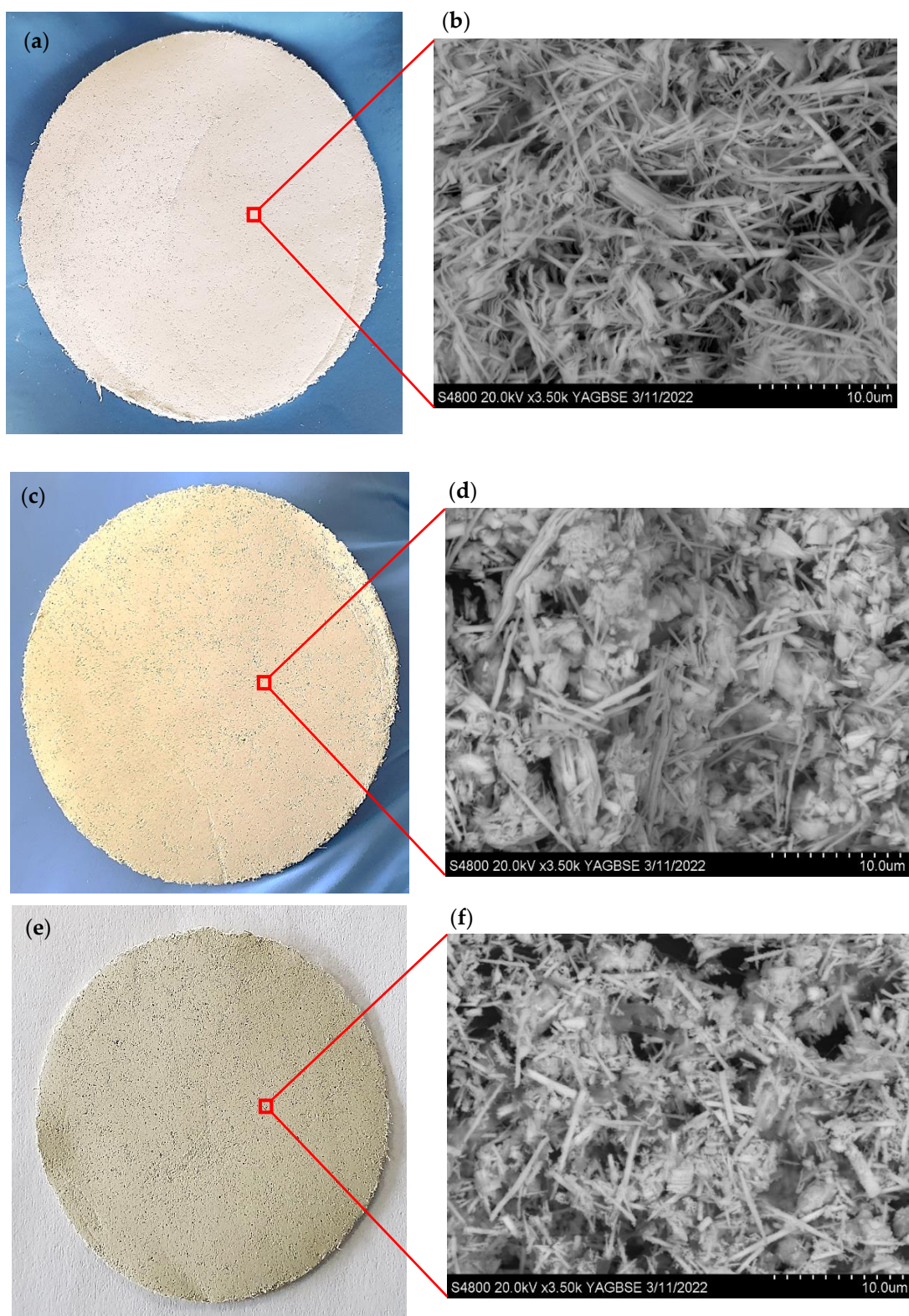


Figure 4. Photographs and SEM images of WO_3 NW/cellulose (a,b) $\text{WO}_3@Fe_2O_3$ /cellulose (c,d) and WO_3 NW@CuO/cellulose (e,f) hybrid membranes.

In order to detect the most significant signals and the presence of Fe_2O_3 and CuO nanoparticles in the membrane structure, EDS investigations were applied. Results of EDS measurements in Table 1 reveal the atomic percentages (at %) of the observed elements in the hybrid membranes. The detected elements of carbon (C), oxygen (O) and tungsten

(W) confirm the presence of cellulose and WO_3 NW in the hybrid membranes, while iron (Fe) and copper (Cu) were related to the deposited Fe_2O_3 and CuO nanoparticles in the membranes. Sodium (Na) was also observed in the membrane analysis, which was a residual material from the preparation procedure of WO_3 NW. EDS analyses that were performed during the TEM and SEM investigations showed good correlations.

Table 1. Elemental (EDS) analysis of raw materials (cellulose and WO_3 NW) and the membranes.

Sample Name	C	O	W	Na	Fe	Cu
Cellulose	45	55	—	—	—	—
WO_3 NW	—	76	24	—	—	—
WO_3 NW/cellulose	36	48	14	2	—	—
WO_3 NW@ Fe_2O_3 /cellulose	33	48	16	2	1	—
WO_3 NW@ CuO /cellulose	31	49	14	2	—	4

2.3. XRD and Specific Surface Area Analysis of Hybrid Membranes

To describe and analyze the crystal structure of the nanocomposites and membranes, XRD investigations were performed. As can be seen in Figure 5a the diffraction peaks at angles $2(\theta^\circ)$ of 19.1° , 33.4° and 44.5° correspond to the reflections from (012), (104), (113) and (113), respectively.

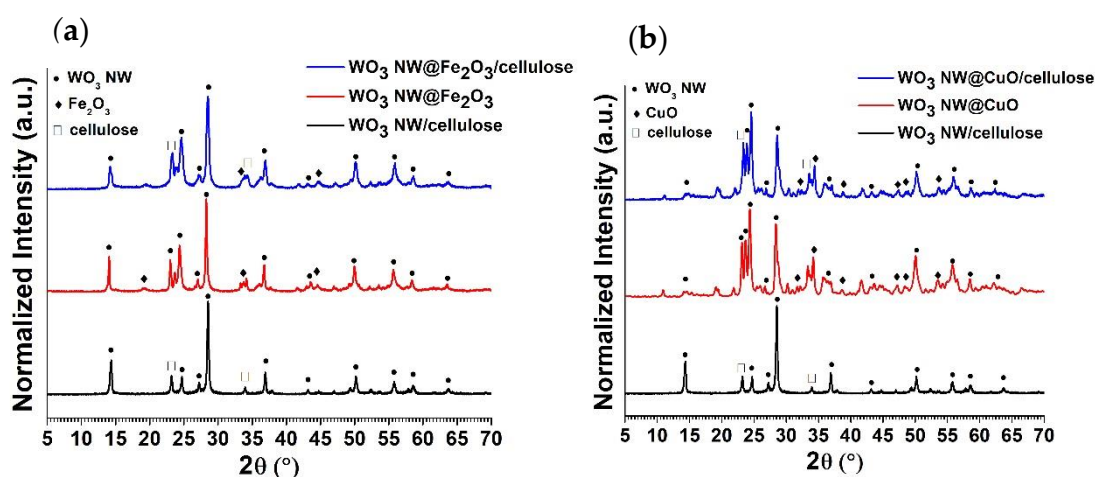


Figure 5. XRD of WO_3 NW@ Fe_2O_3 /cellulose (a), and WO_3 NW@ CuO /cellulose (b) hybrid membranes.

The peaks described above correspond to the hematite ($\alpha\text{-Fe}_2\text{O}_3$) (JCPDS 33-0664). The diffraction peaks at angles $2(\theta^\circ)$ of 14.4° , 24.9° , 28.5° , 36.9° , 43.1° , 50.3° , 55.8° , 58.7° and 63.7° correspond to (100), (110), (200), (201), (300), (220), (202), (400), and (401) reflections, respectively, and relate to the hexagonal structure of WO_3 NW (PDF NO. 75-2187). The diffraction peaks of cellulose (PDF NO. 03-0289) can be identified at angles $2(\theta^\circ)$ of 23.2° and 34.6° , corresponding to the crystal planes of cellulose to (200) and (400) reflections, respectively.

The results of XRD measurements of WO_3 NWs@ CuO /cellulose hybrid membrane are presented in Figure 5b. The diffraction peaks observed at angles $2(\theta^\circ)$ of 32.1° , 34.3° , 38.5° , 47.3° , 48.8° and 53.5° correspond to monoclinic crystal phases of reflections (110), (002), (200), (-112), (-202) and (020), related to copper oxide (CuO) (JCPDS card number 45-0937).

In the next step, a N_2 adsorption technique was applied to determine the specific surface area of the pristine WO_3 NW, the membrane components, and the hybrid membranes. Results are shown in Table 2. There was no significant difference observed between the

surface areas of the obtained hybrid membranes. Both the hybrid membranes had rather low surface areas of approx. 5–8 m²/g.

Table 2. Specific surface area results of the pure materials and the hybrid membranes.

Sample Name	Surface Area (m ² /g)	Pore Diameter (nm)
WO ₃ NW	14	11
cellulose membrane	6	18
Fe ₂ O ₃	62	—
CuO	141	—
WO ₃ NW/cellulose	9	15
WO ₃ NW@Fe ₂ O ₃	7	17
WO ₃ NW@CuO	4	17
WO ₃ NW@Fe ₂ O ₃ /cellulose	8	17
WO ₃ NW@CuO/cellulose	5	17

2.4. Photocatalytic Efficiency of Hybrid Membranes

The photocatalytic activity of the prepared hybrid membranes was measured by studying the removal of methylene blue (MB) under UV light irradiation for 120 min. The results show the maximum degradation efficiency of around 77% for the WO₃@CuO/cellulose membrane. Figure 6 represents the degradation efficiency of different membranes for methylene blue under UV light for 120 min. The efficiency of the WO₃@Fe₂O₃/cellulose membrane and the WO₃/cellulose membrane were almost similar, with an efficiency percentage of 72% and 69%, respectively. Additionally, based on the literature, Fe₂O₃ has a lower photocatalytic activity than CuO [48]; consequently, it can cause an enhanced catalytic performance of the WO₃@CuO/cellulose membrane. In our experiments, high-pressure tanning lamps (Cosmedico[®], Cosmedico, Stuttgart, Germany) were used, which eliminated all possibility of visible-light emission. Consequently, any cut-off filter was not required. In this part, it is mentioned only in general that tungsten oxide can be a suitable material as a photocatalyst that can harness visible light [49] and UV [50] as well, compared to titanium oxide, which is effective only in UV light.

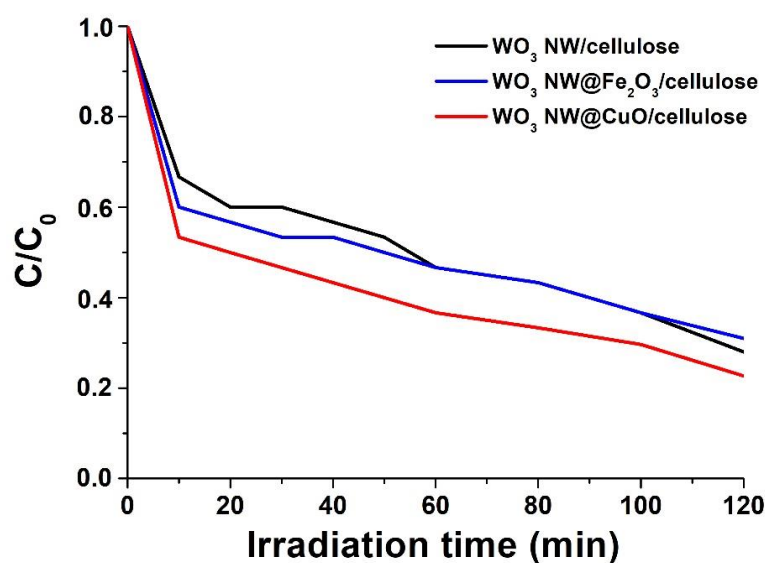


Figure 6. Photocatalytic performance of WO₃ NW/cellulose (black curve), WO₃ NW@Fe₂O₃/cellulose (blue curve), and WO₃ NW@CuO/cellulose (red curve) hybrid membranes in MB degradation reaction.

3. Materials and Methods

3.1. Materials

Sodium tungstate dihydrate ($\text{Na}_2\text{WO}_4 \cdot \text{H}_2\text{O}$) was ordered from Thermo Fisher (Budapest, Hungary), sodium sulfate (Na_2SO_4) was purchased from Lachner Ltd. (Neratovice, Czech Republic), and sodium hydroxide (NaOH) was purchased from Sigma-Aldrich (Budapest, Hungary). Hydrochloric acid (HCl , 37%) and copper (II) acetate monohydrate ($\text{Cu}(\text{OOCCH}_3)_2 \cdot \text{H}_2\text{O}$) were ordered from VWR Chemicals (Debrecen, Hungary). The iron chloride hexahydrate ($\text{FeCl}_3 \cdot 6\text{H}_2\text{O}$) was purchased from Scharlab (Debrecen, Hungary). Cellulose originates from DIPA Ltd. (Miskolc, Hungary). Polyvinylidene (PVDF) filter membranes of a pore size of $0.1 \mu\text{m}$ and a diameter of 47 mm (Durapore-VVLP04700; Sigma Aldrich, Budapest, Hungary) were used for the hybrid membrane preparation.

3.2. Synthesis of WO_3 NanoWires (WO_3 NW)

WO_3 NWs were synthesized using a hydrothermal process in the following procedure. Sodium tungstate (2.5 g) and sodium sulfate (3.0 g) were dissolved in 80 mL of distilled water. HCl (3 M) was added dropwise to the clear solution under continuous stirring, and the pH of the solution was set to 1.5. After 10 min of stirring, the mixture was transferred into a Teflon-lined stainless-steel autoclave for 48 h at 180°C . The product was collected by centrifugation, washed several times with distilled water for neutral pH, then dried at 100°C . Finally, the dried powder was calcinated at 400°C for 1 h.

3.3. Synthesis of WO_3 NW@ Fe_2O_3 /Cellulose Membranes

To produce the WO_3 @ Fe_2O_3 /cellulose hybrid membranes (Figure 7), firstly, the WO_3 NW@ Fe_2O_3 nanocomposite material was synthesized. Hence, a homogeneous solution was prepared by the usage of a certain amount of $\text{FeCl}_3 \cdot 6\text{H}_2\text{O}$ precursor and 100 mL of distilled water. Secondly, 0.95 g of WO_3 NWs were added to the solution and stirred for 1 h. To adjust the pH in the basic range, NaOH was added dropwise to the solution, and after that the solution was placed into an autoclave for 9 h at 90°C . As-prepared material was washed with distilled water for pH 7, dried for 12 h at 50°C and finally it was heat-treated for 2 h at 500°C in a static furnace. The amount of the Fe_2O_3 nanoparticles in the product was 5 w/w%. For membrane preparation, 0.2 g from the produced WO_3 NW@ Fe_2O_3 nanocomposite powder was dispersed in 100 mL of EtOH for 1 h, then 5 g of cellulose solution (1 w/w%) was added to the solution and stirred for 1 h. To obtain self-supported hybrid membranes, the vacuum filtration technique was applied through a PVDF membrane (total mass of 250 mg/membrane). Finally, the membranes were dried in a furnace for 30 min at 40°C .

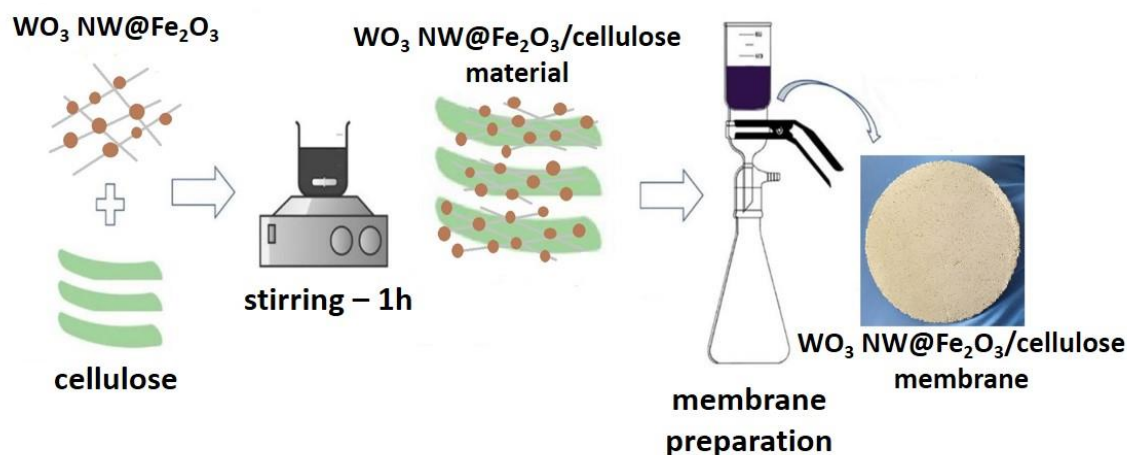


Figure 7. Schematic illustration of the process of hybrid membrane preparation.

3.4. Synthesis of WO₃ NW@CuO/Cellulose Membranes

Similarly, a certain amount of (Cu(CH₃COO)₂ · H₂O) was dissolved in 100 mL of EtOH and left under vigorous stirring for 30 min. Secondly, 0.95 g of WO₃ NW was added directly to the solution, and stirred continuously for 1 h. After that, the as-prepared material was placed into a stainless-steel autoclave and put into a static furnace at 150 °C for 12 h. The product thus obtained was collected and washed, then calcinated for 2 h at 500 °C. The CuO nanoparticle load in the final composition was 5% by weight. For the membrane preparation, 0.2 g from the produced WO₃ NW@CuO nanocomposite powder was dispersed in 100 mL of EtOH for 1 h, then 5 g of the cellulose solution (1 w/w%) was added to the solution and stirred for 1 h. To obtain self-supported hybrid membranes, the vacuum filtration technique was applied through a PVDF membrane (total mass of 250 mg/membrane). Finally, the membranes were dried in a furnace for 30 min at 40 °C.

3.5. Characterization Techniques

To analyze the morphology of the synthesized WO₃ NW@Fe₂O₃ and WO₃ NW@CuO nanocomposites, high-resolution transmission electron microscopy (FEI Technai G² F20 HRTEM, Hillsboro, OR, USA) was used. To prepare TEM grids, powder samples were dispersed in ethanol and sonicated for 5 min. On a Cu TEM grid (300 mesh copper grids, lacey carbon, Ted Pella Inc.), a droplet of suspension was placed. To determine the diameter of the materials ImageJ software (Java 1.8.0, Wisconsin, WI, USA, 2020) was applied, utilizing HRTEM images and the original scale bar. The elemental compositions of the WO₃ NW@Fe₂O₃ and the WO₃ NW@CuO nanocomposites were investigated by energy-dispersive X-ray spectroscopy (EDS; AMETEK Inc., Berwyn, PA, USA; active area 30 mm²) coupled to the HRTEM instrument.

The crystal structure of the hybrid membranes was determined using X-ray powder diffraction (XRD) (Rigaku Miniflex diffractometer; Rigaku, Austin, TX, USA) at (CuK α = 0.15418 nm) (40 kV and 40 mA) in a parallel beam geometry (Göbel mirror) with a position-sensitive detector (Vantec1, 1° opening). On top-loaded specimens in zero-background Si sample containers, measurements were made in the 2–80° (2 Theta) range using a 0.007° (2 Theta)/14 sec goniometer speed.

For surface morphology investigation, we used a scanning electron microscopy technique. In the case of the hybrid membranes, SEM investigations and EDS spectroscopy were carried out with a Hitachi S-4700 Type II FE-SEM (Hitachi, Tokyo, Japan), operating in the range of 0–30 keV, while the images of the pristine WO₃ NW were recorded with a Thermo Helios G4 PFIB CXe instrument (Thermo Fisher, Eindhoven, The Netherlands). Typical EDS maps and spectra were acquired using Acceleration Voltage values between 10 kV and 25 kV, with a take-off angle of 35° and a dwell time of 200 ms. For SEM analysis, powders were deposited on a sticky carbon tape. Each sample, such as powders and membranes, was observed directly without any conductive coating. The typical SEM working distance was 5 mm and acceleration voltage ranged from 2 kV up to 25 kV, depending on the image quality and charging conditions.

To determine the surface area of the raw materials, the nanocomposites and the hybrid membranes, nitrogen adsorption-desorption experiments were carried out at 77 K to determine the Brunauer-Emmett-Teller (BET)-specific surface area using an ASAP 2020 instrument (Micromeritics Instrument Corp. Norcross, GA, USA).

3.6. Photocatalytic Experiments

The photocatalytic activity of the as-prepared hybrid materials was investigated in the decomposition reactions of methylene blue (MB). Firstly, each membrane was placed into a solution of MB (100 mL of 0.03 mM) and kept in darkness for two hours to attain adsorption-desorption equilibrium. After this, the solution was exposed to UV-A lamps (300–500 W, Cosmedico N 400 R7S; Cosmedico, Stuttgart, Germany) for 120 min. The samples were withdrawn at regular time intervals, followed by centrifugation and filtration. The decrease in MB concentration was analyzed by using a UV-vis spectrophotometer (BEL

UV-M51; Bel Engineering, Monza, Italy). The removal efficiency of the membranes was measured by recording the absorbance at 664 nm and the degradation efficiency (% deg.) was calculated using the following formula:

$$\% \text{deg.} = \frac{(C_0 - C_t)}{C_0} \times 100 \quad (1)$$

where C_0 is initial concentration at time $t = 0$, C_t is the concentration at time “ t ” and % deg. is the photodegradation efficiency of the materials for MB removal.

4. Conclusions

In this study, the development of novel WO_3 nanowire-based hybrid membranes and their photocatalytic properties for the decomposition of methylene blue under UV light is presented. The as-prepared WO_3 NW@ Fe_2O_3 /cellulose and WO_3 NW@CuO/cellulose membranes were characterized by HRTEM, SEM, EDS and XRD instruments. Based on these investigations, it was found that the preparation of pristine WO_3 NW, WO_3 NW@ Fe_2O_3 , WO_3 NW@CuO nanocomposites and the production of hybrid membranes was successful.

The results of photocatalytic experiments showed that both types of hybrid membranes have a good ability to decompose MB in 120 min of UV irradiation. The photocatalytic degradation efficiency for MB removal by WO_3 @ Fe_2O_3 /cellulose was 72%, while up to 77% was achieved in the case of WO_3 @CuO/cellulose membrane. Comparing the obtained results, in our recently published paper [51] it was found that in both cases the CuO-decorated nanowires (WO_3 and TiO_2) provided the highest removal efficiency. Furthermore, it can also be stated that the usage of nanowire-based membranes could be a promising direction in the field of water treatment technologies. Since we applied UV light in this study, presumably significant degradation could be also observed under visible light irradiation; therefore, we intend to explore these questions in a further study.

Moreover, one more study will be reported in the near future about the microbiological and toxicological properties of these hybrid membranes. We hope that by exploiting the advantageous properties of the nanowire-based membranes presented here, sustainable solutions could be opened in the field of water treatment technologies.

Author Contributions: Conceptualization, M.A.S., and N.S.; methodology, N.S., and Z.N.; validation, M.A.S., N.S.; investigation, G.K., I.K., and N.S.; writing—original draft preparation, M.A.S., N.S., L.N.; Z.N.; writing—review and editing, K.H., and Z.N.; visualization, K.H., and Z.N., supervision, K.H., and Z.N.; project administration, Z.N.; funding acquisition, Z.N. All authors have read and agreed to the published version of the manuscript.

Funding: This research was funded by the National Research, Development and Innovation Office (NRDI Fund), grant number 2020-2.1.1-ED-2020-00029, Hungary and the experimental data used in this research were generated through access to the JRC Nanobiotechnology Laboratory under the Framework of access to the Joint Research Centre Physical Research Infrastructures of the European Commission (Virimmo project, Research Infrastructure Access Agreement N° 36171/11).

Data Availability Statement: Not applicable.

Acknowledgments: Z. Németh would like to thank the Hungarian Academy of Sciences Bolyai János Research Scholarship Program.

Conflicts of Interest: The authors declare no conflict of interest.

References

1. Bexfield, L.M.; Toccalino, P.L.; Belitz, K.; Foreman, W.T.; Furlong, E.T. Hormones and Pharmaceuticals in Groundwater Used As a Source of Drinking Water Across the United States. *Environ. Sci. Technol.* **2019**, *53*, 2950–2960. [[CrossRef](#)] [[PubMed](#)]
2. Al-Tohamy, R.; Ali, S.S.; Li, F.; Okasha, K.M.; Mahmoud, Y.A.-G.; Elsamahy, T.; Jiao, H.; Fu, Y.; Sun, J. A critical review on the treatment of dye-containing wastewater: Ecotoxicological and health concerns of textile dyes and possible remediation approaches for environmental safety. *Ecotoxicol. Environ. Saf.* **2022**, *231*, 113160. [[CrossRef](#)] [[PubMed](#)]

3. Wang, J.; Zhuan, R. Degradation of antibiotics by advanced oxidation processes: An overview. *Sci. Total Environ.* **2019**, *701*, 135023. [[CrossRef](#)] [[PubMed](#)]
4. Poerio, T.; Piacentini, E.; Mazzei, R. Membrane Processes for Microplastic Removal. *Molecules* **2019**, *24*, 4148. [[CrossRef](#)] [[PubMed](#)]
5. Karpińska, J.; Kotowska, U. Removal of Organic Pollution in the Water Environment. *Water* **2019**, *11*, 2017. [[CrossRef](#)]
6. Crini, G.; Lichtfouse, E. Advantages and disadvantages of techniques used for wastewater treatment. *Environ. Chem. Lett.* **2019**, *17*, 145–155. [[CrossRef](#)]
7. Etacheri, V.; Di Valentin, C.; Schneider, J.; Bahnemann, D.; Pillai, S.C. Visible-light activation of TiO₂ photocatalysts: Advances in theory and experiments. *J. Photochem. Photobiol. C Photochem. Rev.* **2015**, *25*, 1–29. [[CrossRef](#)]
8. Carp, O.; Huisman, C.L.; Reller, A. Photoinduced reactivity of titanium dioxide. *Prog. Solid State Chem.* **2004**, *32*, 33–177. [[CrossRef](#)]
9. Zhang, F.; Wang, X.; Liu, H.; Liu, C.; Wan, Y.; Long, Y.; Cai, Z. Recent Advances and Applications of Semiconductor Photocatalytic Technology. *Appl. Sci.* **2019**, *9*, 2489. [[CrossRef](#)]
10. Santos, R.K.; Martins, T.A.; Silva, G.N.; Conceição, M.V.S.; Nogueira, I.C.; Longo, E.; Botelho, G. Ag₃PO₄ /NiO composites with enhanced photocatalytic activity under visible light. *ACS Omega* **2020**, *5*, 21651–21661. [[CrossRef](#)]
11. Liao, C.; Ma, Z.; Chen, X.; He, X.; Qiu, J. Controlled synthesis of bismuth oxyiodide toward optimization of photocatalytic performance. *Appl. Surf. Sci.* **2016**, *387*, 1247–1256. [[CrossRef](#)]
12. Sharma, N.; Pap, Z.; Garg, S.; Hernadi, K. Photocatalyst Composites from Bi-based and Carbon Materials for Visible Light Photodegradation. In *Green Photocatalytic Semiconductors*; Springer: Cham, Switzerland, 2022; pp. 145–178. [[CrossRef](#)]
13. Castillo-Cabrera, G.X.; Espinoza-Montero, P.J.; Alulema-Pullupaxi, P.; Mora, J.R.; Villacís-García, M.H. Bismuth Oxyhalide-Based Materials (BiOX: X = Cl, Br, I) and Their Application in Photoelectrocatalytic Degradation of Organic Pollutants in Water: A Review. *Front. Chem.* **2022**, *10*. [[CrossRef](#)] [[PubMed](#)]
14. Yu, Y.; Wu, S.; Gu, J.; Liu, R.; Wang, Z.; Chen, H.; Jiang, F. Visible-light photocatalytic degradation of bisphenol A using cobalt-to-oxygen doped graphitic carbon nitride with nitrogen vacancies via metal-to-ligand charge transfer. *J. Hazard. Mater.* **2020**, *384*, 121247. [[CrossRef](#)] [[PubMed](#)]
15. Liu, C.; Lü, H.; Yu, C.; Ding, B.; Ye, R.; Ji, Y.; Dai, B.; Liu, W. Novel FeWO₄/WO₃ nanoplate with p-n heterostructure and its enhanced mechanism for organic pollutants removal under visible-light illumination. *J. Environ. Chem. Eng.* **2020**, *8*, 104044. [[CrossRef](#)]
16. Fakhri, A.; Behrouz, S. Photocatalytic properties of tungsten trioxide (WO₃) nanoparticles for degradation of Lidocaine under visible and sunlight irradiation. *Sol. Energy* **2015**, *112*, 163–168. [[CrossRef](#)]
17. Samuel, O.; Othman, M.H.D.; Kamaludin, R.; Sinsamphanh, O.; Abdullah, H.; Puteh, M.H.; Kurniawan, T.A. WO₃-based photocatalysts: A review on synthesis, performance enhancement and photocatalytic memory for environmental applications. *Ceram. Int.* **2021**, *48*, 5845–5875. [[CrossRef](#)]
18. Zhou, J.; Ding, Y.; Deng, S.Z.; Gong, L.; Xu, N.S.; Wang, Z.L. Three-Dimensional Tungsten Oxide Nanowire Networks. *Adv. Mater.* **2005**, *17*, 2107–2110. [[CrossRef](#)]
19. Szilágyi, I.M.; Fórizs, B.; Rosseler, O.; Szegedi, Á.; Németh, P.; Király, P.; Tárkányi, G.; Vajna, B.; Varga-Josepovits, K.; László, K.; et al. WO₃ photocatalysts: Influence of structure and composition. *J. Catal.* **2012**, *294*, 119–127. [[CrossRef](#)]
20. Zheng, H.; Ou, J.Z.; Strano, M.S.; Kaner, R.B.; Mitchell, A.; Kalantar-Zadeh, K. Nanostructured Tungsten Oxide-Properties, Synthesis, and Applications. *Adv. Funct. Mater.* **2011**, *21*, 2175–2196. [[CrossRef](#)]
21. Yao, S.; Qu, F.; Wang, G.; Wu, X. Facile hydrothermal synthesis of WO₃ nanorods for photocatalysts and supercapacitors. *J. Alloys Compd.* **2017**, *724*, 695–702. [[CrossRef](#)]
22. Jamali, M.; Tehrani, F.S. Effect of synthesis route on the structural and morphological properties of WO₃ nanostructures. *Mater. Sci. Semicond. Process.* **2019**, *107*, 104829. [[CrossRef](#)]
23. Wang, H.-R.; Zhang, G.-Y.; Xu, Y.-Y.; Wei, X.-M.; Shen, X.-Q.; Sun, Y.-Q. Facile ethanol/water solvothermal synthesis of {001} facet oriented WO₃ architectures with superior simulated sunlight photocatalytic activities. *CrystEngComm* **2016**, *18*, 8089–8100. [[CrossRef](#)]
24. Parthibavarman, M.; Karthik, M.; Prabhakaran, S. Facile and one step synthesis of WO₃ nanorods and nanosheets as an efficient photocatalyst and humidity sensing material. *Vacuum* **2018**, *155*, 224–232. [[CrossRef](#)]
25. Ahmed, B.; Kumar, S.; Ojha, A.K.; Donfack, P.; Materny, A. Facile and controlled synthesis of aligned WO₃ nanorods and nanosheets as an efficient photocatalyst material. *Spectrochim. Acta Part A Mol. Biomol. Spectrosc.* **2017**, *175*, 250–261. [[CrossRef](#)]
26. Navarrete-Magaña, M.; Estrella-González, A.; May-Ix, L.; Cipagauta-Díaz, S.; Gómez, R. Improved photocatalytic oxidation of arsenic (III) with WO₃/TiO₂ nanomaterials synthesized by the sol-gel method. *J. Environ. Manag.* **2021**, *282*, 111602. [[CrossRef](#)]
27. Martínez-de la Cruz, A.; Martínez, D.S.; Cuéllar, E.L. Synthesis and characterization of WO₃ nanoparticles prepared by the precipitation method: Evaluation of photocatalytic activity under vis-irradiation. *Solid State Sci.* **2010**, *12*, 88–94. [[CrossRef](#)]
28. Mohammadi, S.; Sohrabi, M.; Golikand, A.N.; Fakhri, A. Preparation and characterization of zinc and copper co-doped WO₃ nanoparticles: Application in photocatalysis and photobiology. *J. Photochem. Photobiol. B Biol.* **2016**, *161*, 217–221. [[CrossRef](#)] [[PubMed](#)]
29. Galstyan, V.; Poli, N.; D’Arco, A.; Macis, S.; Lupi, S.; Comini, E. A novel approach for green synthesis of WO₃ nanomaterials and their highly selective chemical sensing properties. *J. Mater. Chem. A* **2020**, *8*, 20373–20385. [[CrossRef](#)]

30. Nayak, A.K.; Sohn, Y.; Pradhan, D. Facile green synthesis of $\text{WO}_3 \cdot \text{H}_2\text{O}$ nanoplates and WO_3 nanowires with enhanced photoelectrochemical performance. *Cryst. Growth Des.* **2017**, *17*, 4949–4957. [[CrossRef](#)]
31. Manjunatha, A.; Pavithra, N.; Shivanna, M.; Nagaraju, G.; Ravikumar, C. Synthesis of Citrus Limon mediated SnO_2 - WO_3 nanocomposite: Applications to photocatalytic activity and electrochemical sensor. *J. Environ. Chem. Eng.* **2020**, *8*, 104500. [[CrossRef](#)]
32. Nagy, D.; Szilágyi, I.M.; Fan, X. Effect of the morphology and phases of WO_3 nanocrystals on their photocatalytic efficiency. *RSC Adv.* **2016**, *6*, 33743–33754. [[CrossRef](#)]
33. Senthil, R.A.; Priya, A.; Theerthagiri, J.; Selvi, A.; Nithyadharseni, P.; Madhavan, J. Facile synthesis of α - $\text{Fe}_2\text{O}_3/\text{WO}_3$ composite with an enhanced photocatalytic and photo-electrochemical performance. *Ionics* **2018**, *24*, 3673–3684. [[CrossRef](#)]
34. Ikram, M.; Umar, E.; Raza, A.; Haider, A.; Naz, S.; Ul-Hamid, A.; Haider, J.; Shahzadi, I.; Hassan, J.; Ali, S. Dye degradation performance, bactericidal behavior and molecular docking analysis of Cu-doped TiO_2 nanoparticles. *RSC Adv.* **2020**, *10*, 24215–24233. [[CrossRef](#)]
35. Huang, Z.-F.; Song, J.; Pan, L.; Zhang, X.; Wang, L.; Zou, J.-J. Tungsten Oxides for Photocatalysis, Electrochemistry, and Phototherapy. *Adv. Mater.* **2015**, *27*, 5309–5327. [[CrossRef](#)] [[PubMed](#)]
36. Dursun, S.; Koyuncu, S.N.; Kaya, I.C.; Kaya, G.G.; Kalem, V.; Akyildiz, H. Production of CuO-WO_3 hybrids and their dye removal capacity/performance from wastewater by adsorption/photocatalysis. *J. Water Process Eng.* **2020**, *36*, 101390. [[CrossRef](#)]
37. Huang, Y.; Guo, Z.; Liu, H.; Zhang, S.; Wang, P.; Lu, J.; Tong, Y. Heterojunction Architecture of N-Doped WO_3 Nanobundles with Ce_2S_3 Nanodots Hybridized on a Carbon Textile Enables a Highly Efficient Flexible Photocatalyst. *Adv. Funct. Mater.* **2019**, *29*, 1903490. [[CrossRef](#)]
38. Hitam, C.; Jalil, A. A review on exploration of Fe_2O_3 photocatalyst towards degradation of dyes and organic contaminants. *J. Environ. Manag.* **2020**, *258*, 110050. [[CrossRef](#)] [[PubMed](#)]
39. Dulta, K.; Ağçeli, G.K.; Chauhan, P.; Jasrotia, R.; Ighalo, J.O. Multifunctional CuO nanoparticles with enhanced photocatalytic dye degradation and antibacterial activity. *Sustain. Environ. Res.* **2022**, *32*, 2. [[CrossRef](#)]
40. Karthikeyan, C.; Arunachalam, P.; Ramachandran, K.; Al-Mayouf, A.M.; Karuppuchamy, S. Recent advances in semiconductor metal oxides with enhanced methods for solar photocatalytic applications. *J. Alloys Compd.* **2020**, *828*, 154281. [[CrossRef](#)]
41. Leong, S.; Razmjou, A.; Wang, K.; Hapgood, K.; Zhang, X.; Wang, H. TiO_2 based photocatalytic membranes: A review. *J. Membr. Sci.* **2014**, *472*, 167–184. [[CrossRef](#)]
42. Pang, X.; Xue, S.; Zhou, T.; Xu, Q.; Lei, W. 2D/2D nanohybrid of Ti_3C_2 MXene/ WO_3 photocatalytic membranes for efficient water purification. *Ceram. Int.* **2021**, *48*, 3659–3668. [[CrossRef](#)]
43. Kim, J.; Van der Bruggen, B. The use of nanoparticles in polymeric and ceramic membrane structures: Review of manufacturing procedures and performance improvement for water treatment. *Environ. Pollut.* **2010**, *158*, 2335–2349. [[CrossRef](#)] [[PubMed](#)]
44. Asiri, A.M.; Pugliese, V.; Petrosino, F.; Khan, S.B.; Alamry, K.A.; Alfifi, S.Y.; Marwani, H.M.; Alotaibi, M.M.; Mukherjee, D.; Chakraborty, S. Photocatalytic Degradation of Textile Dye on Blended Cellulose Acetate Membranes. *Polymers* **2022**, *14*, 636. [[CrossRef](#)] [[PubMed](#)]
45. Santos, E.N.; Ágoston, Á.; Kertész, S.; Hodúr, C.; László, Z.; Pap, Z.; Kása, Z.; Alapi, T.; Krishnan, S.G.; Arthanareeswaran, G.; et al. Investigation of the applicability of TiO_2 , BiVO_4 , and WO_3 nanomaterials for advanced photocatalytic membranes used for oil-in-water emulsion separation. *Asia-Pac. J. Chem. Eng.* **2020**, *15*, e2549. [[CrossRef](#)]
46. Warsi, A.-Z.; Aziz, F.; Zulfiqar, S.; Haider, S.; Shakir, I.; Agboola, P.O. Synthesis, Characterization, Photocatalysis, and Antibacterial Study of WO_3 , MXene and WO_3/MXene Nanocomposite. *Nanomaterials* **2022**, *12*, 713. [[CrossRef](#)] [[PubMed](#)]
47. Duan, G.; Chen, L.; Jing, Z.; Luna, P.D.; Wen, L.; Zhang, L.; Zhao, L.; Xu, J.; Li, Z.; Yang, Z.; et al. Robust antibacterial activity of tungsten oxide (WO_{3-x}) nanodots. *Chem. Res. Toxicol.* **2019**, *32*, 1357–1366. [[CrossRef](#)]
48. Asenath-Smith, E.; Ambrogi, E.K.; Barnes, E.; Brame, J.A. CuO enhances the photocatalytic activity of Fe_2O_3 through synergistic reactive oxygen species interactions. *Colloids Surfaces A Physicochem. Eng. Asp.* **2020**, *603*, 125179. [[CrossRef](#)]
49. Bai, S.; Zhang, K.; Sun, J.; Luo, R.; Li, D.; Chen, A. Surface decoration of WO_3 architectures with Fe_2O_3 nanoparticles for visible-light-driven photocatalysis. *CrystEngComm* **2014**, *16*, 3289–3295. [[CrossRef](#)]
50. Lima, M.S.; Cruz-Filho, J.F.; Noletto, L.F.; Silva, L.J.; Costa, T.M.; Luz, G.E. Synthesis, characterization and catalytic activity of $\text{Fe}_3\text{O}_4@/\text{WO}_3/\text{SBA-15}$ on photodegradation of the acid dichlorophenoxyacetic (2,4-D) under UV irradiation. *J. Environ. Chem. Eng.* **2020**, *8*, 104145. [[CrossRef](#)]
51. Shehab, M.A.; Sharma, N.; Valsesia, A.; Karacs, G.; Kristály, F.; Koós, T.; Leskó, A.K.; Nánai, L.; Hernadi, K.; Németh, Z. Preparation and Photocatalytic Performance of TiO_2 Nanowire-Based Self-Supported Hybrid Membranes. *Molecules* **2022**, *27*, 2951. [[CrossRef](#)]